Journal of Magnetism and Magnetic Materials 446 (2018) 1–6

Contents lists available at ScienceDirect

Journal of Magnetism and Magnetic Materials

journal homepage: www.elsevier.com/locate/jmmm

Research articles

Spin-wave resonances of ferromagnetic films with spatially modulated anisotropy

M.V. Sapozhnikov *, R.V. Gorev, E.A. Karashtin, V.L. Mironov

Institute for Physics of Microstructures RAS, Nizhny Novgorod 603950, GSP-105, Russia

ARTICLE INFO

Article history:
Received 17 April 2017
Received in revised form 27 August 2017
Accepted 1 September 2017
Available online 5 September 2017

Keywords:
Magnetic skyrmion
Ferromagnetic resonance
Perpendicular anisotropy
Nonuniform spin-wave resonances

ABSTRACT

We study the dynamical properties of a magnetic film with spatially modulated perpendicular anisotropy by numerical simulations. Both topologically charged states (magnetic skyrmions) and uncharged uniform and nonuniform states are considered. The dependences of the ferromagnetic resonance (FMR) spectra on the geometry and material parameters of the system are analyzed. It is found that the spectra contain resonances of the localized and delocalized modes of the magnetization oscillations. In the case of nonuniform states the localized modes have the form of rotating magnetization distributions. The direction of the rotation depends on the local density of the toroidal moment of the state. The magnetic states with different FMR spectra can be easily switched by a temporary applying of a uniform external magnetic field that can be used in the tunable microwave devices.

1. Introduction

Soliton-like magnetization distributions carrying topological charge in magnetic materials are well known since the late 1970s [1,2]. The new rise of the interest to this topic is caused by experimental observation of the topological solitons in the chiral magnets [3–5]. In the case if the direction of magnetic moment of the soliton varies continuously and wraps around a unit sphere the soliton has the topology of a 2D skyrmion. The topological nature of such states affects dynamics of conduction electrons causing unusual spin-electronic properties of skyrmions, such as topological Hall effect [6–9], current-driven motion in ultra-low currents [10,11] and also intrinsic magnetoelectric coupling [12]. Due to these unique characteristics the skyrmions have huge potential to be exploited for spin-based high-dense information storage and processing integrated in the same device [13]. Recently the dynamical properties of the magnetic skyrmions in the alternating electromagnetic fields were also studied because of their potential application in microwave devices. The most attention in this way is paid to the skyrmions naturally stabilized by the Dzyaloshinskii-Moriya interaction (DMI) in the non-centrosymmetric magnetic materials [14–18]. On the other side the skyrmion states can be stabilized even without DMI by the proper spatial nanostructuring of the magnetic films with perpendicular anisotropy. It can be realized by periodical modulation of the magnetic film thickness [19] or its material parameters, for example value of anisotropy [20,21]. Evidently the radio frequency (RF) resonance properties of this system should be different in comparison with DMI-stabilized skyrmion lattices. Besides, nanostructuring opens additional opportunities to artificially tune the RF properties of this system. Our investigation is also inspired by recent development of the novel possibilities for the local measurements of the nonuniform FMR modes in magnetic nanostructures by magnetic resonance force microscopy [22–24].

Here we study the RF dynamical properties of the artificial skyrmion lattices stabilized in the film with spatially modulated perpendicular anisotropy by means of micromagnetic simulations. The aim of our work is to answer two questions. (1) How could the RF properties of this system be tuned by changing geometry and material parameters of the structure? (2) Is there an easy way to control the RF spectra of the system by changing its magnetic configuration? The answers will help to understand the ways of utilization of the artificial skyrmion lattices in the microwave devices.

2. Micromagnetic simulation

The micromagnetic modeling is performed using Object Oriented MicroMagnetic Framework (OOMMF) software [25] based on a numerical solution of the system of Landau-Lifshitz-Gilbert (LLG) equations for the magnetization:

* Corresponding author.
E-mail address: msap@ipmras.ru (M.V. Sapozhnikov).

http://dx.doi.org/10.1016/j.jmmm.2017.09.006
0304-8853/

$$\frac{\partial \mathbf{M}}{\partial t} = -\gamma[\mathbf{M} \times \mathbf{H}_{eff}] + \frac{\alpha}{M_s}\left[\mathbf{M} \times \frac{\partial \mathbf{M}}{\partial t}\right], \quad (1)$$

where **M** is the magnetization, γ is the gyromagnetic ratio, α is the dimensionless damping parameter, and M_s is the magnetization at saturation. The effective field

$$\mathbf{H}_{eff} = -\frac{\partial E}{\partial \mathbf{M}}, \quad (2)$$

is a variation derivative of the energy. According to the Eq. (1) in the limit of small dumping the value of the effective field determines the frequency of the ferromagnetic resonance as

$$\omega = \gamma H_{eff}. \quad (3)$$

Usually the total energy E of the magnetic system is defined as

$$E = E_h + E_{ex} + E_{dem} + E_a. \quad (4)$$

Here E_h is the energy of the interaction between the magnetization and an external magnetic field, E_{ex} is the energy of the exchange interaction, E_{dem} is the demagnetization energy of the system and E_a is the energy of the magnetic anisotropy. Expressions for these terms have a conventional form [26,27]. In the simulations the geometric configuration and the material parameters of the system are chosen correspondingly to the recent experiments [21] where the dense artificial skyrmion lattice is observed. The considered system is the magnetic film with perpendicular anisotropy which value is locally decreased in some areas. The areas with the decreased anisotropy are the circular spots arranged in the rectangular lattice (Fig. 1). In the simulations we use an elementary cell of such lattice infinitely extended in the plane using 2D periodic boundary conditions. The circular area with the changed anisotropy is located in the elementary cell center and has the diameter twice less than the cell size. The film thickness is 7.5 nm, the elementary cell size is 100 or 200 nm, so the area with the reduced anisotropy has the diameter 50 or 100 nm respectively. The material parameters for simulation correspond to Co/Pt multilayers [21], the magnetization in saturation M_s = 200 G, the initial uniaxial anisotropy of the film $K_0 = 3.65 \times 10^5$ erg/cm^3, and the exchange coefficient $A = 2.5 \times 10^{-8}$ erg/cm. The chosen value of the anisotropy coefficient corresponds to the easy-axis direction of the magnetization in the film. The simulation grid size of $2.5 \times 2.5 \times 7.5$ nm^3 is less than the exchange length.

Whereas the anisotropy of the film should be perpendicular to realize skyrmion lattice, the anisotropy in the spot can vary in wide ranges. If it is still perpendicular the skyrmion takes the form of the small magnetic bubble domain (denoted as MB in Fig. 1b). We simulate this situation for two values of K_1 equal to 2.8×10^5 erg/cm^3 and 2.4×10^5 erg/cm^3. This allows us to study the influence of the anisotropy value on the FMR spectra of the system.

For the smaller K_1 when the effective anisotropy (together with demagnetizing) becomes of the easy plain type, the topologically charged skyrmionic state can be realized as a vortex inside the central spot surrounded by perpendicularly magnetized film. If the vortex core is directed oppositely to the film magnetization (denoted as OV in Fig. 1b) it carries the topological charge equal to + 1. Vice versa the topological charge of the system is equal to zero if the vortex core is codirectional to the film magnetization (denoted as CV in Fig. 1b). So this codirectional vortex is not a skyrmion [20].

These states of the system are simulated with $K_1 = 10^5$ erg/cm^3. The magnetization is supposed to be uniform in the perpendicular direction. All simulated magnetic states are represented in Fig. 1. For the reference we name examined states as "uniform" (UN), "magnetic bubble" (MB), "opposite magnetic vortex" (OV), and "co-directional vortex" (CV). There are the schematic pictures of the magnetization configuration as well as the distribution of the topological charge density in the corresponding state. The topological charge density is defined as [7]

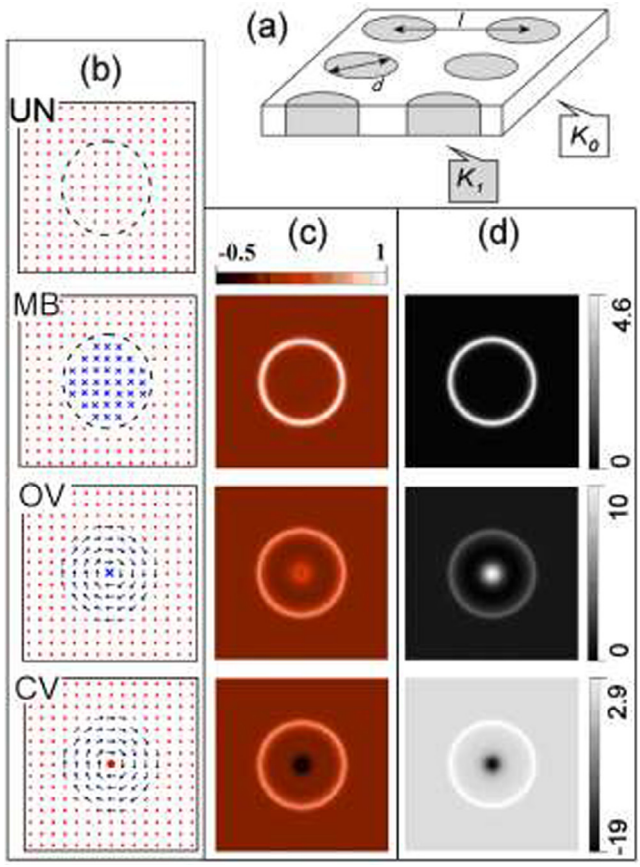

Fig. 1. (a) The geometry of the simulated system. The spots with the reduced anisotropy (diameter d) form a rectangular lattice (period l). (b) Four possible magnetization configurations of the system. UN is uniform state, MB is magnetic bubble, OV is opposite vortex (magnetization of the core is opposite to the film magnetization), CV is co-directional vortex (magnetization of the core is codirectional to the film magnetization). Points (red) and crosses (blue) denote the magnetic moments directed perpendicular to the film plain in the opposite directions (up and down respectively). Dashed circle is the boundary of the central area. (c) The distributions of the toroidal moment density .in the MB, OV and CV states respectively. (d) Distributions of the topological charge density (in 10^{-4}) of the same states. (For interpretation of the references to colour in this figure legend, the reader is referred to the web version of this article.)

$$\phi(x,y) = \frac{1}{4\pi}\mathbf{n}\frac{\partial \mathbf{n}}{\partial x} \times \frac{\partial \mathbf{n}}{\partial y}, \quad (5)$$

where $\mathbf{n} = \mathbf{M}(r)/|\mathbf{M}(r)|$ is the unit vector of local orientation of the magnetization. Evidently in the case of the uniform state $\phi \equiv 0$. The topological charge defined as the integral of the topological charge density ϕ (x,y) over the system surface is equal to 1 for MB and OV, so they are skyrmions [20]. In these two states the magnetization is continuously changed from up direction in the center to down at the periphery in all radial directions away from the center. It wraps a sphere pointing in all directions as it is usual for the 2D magnetic skyrmion. In the case of the MB the skyrmion charge density is concentrated near the 180° Bloch domain wall, while in the case of the OV the topological charge is the sum of vortex core topological charge (1/2) and the charge of 90° domain wall between the vortex and the periphery (also 1/2). In the CV the topological charge of vortex core (1/2) is totally compensated by the topological charge of wall between the vortex and the periphery (−1/2). So CV is topologically uncharged state. It can be continuously deformed to the uniform state where $\phi \equiv 0$ in every point.

Another important characteristic of the magnetic states in the considered system is the distribution of local density of toroidal moment. It is known that the presence of the toroidal moment in magnetic system leads to the nonreciprocal propagation of spin waves in "forward"/"backward" (or "plus φ"/"minus φ") directions [28,29]. Here, the local density of toroidal moment can be written as curl **M**. The φ-component of this vector lies in the plane of the system and so can lead to the nonreciprocity of spin-waves propagation. As well as the scalar topological charge density the vector toroidal moment density results from noncomplanar distribution of the magnetization in the examined states. So they are well correlated in the system as it is seen from Fig. 1c, d.

The following algorithm of simulations is used in our work. At the first stage the system relaxes to the chosen UN, NB, OV or CV state at zero external field. After that the AC external field is applied and the amplitude of the stationary oscillations of the average magnetization of the system

$$\boldsymbol{m} = (m_x^2 + m_y^2 + m_z^2)^{1/2} \tag{6}$$

is calculated. The AC field is directed in the plane of the system along the elementary cell side, its amplitude is 1 Oe, the dumping constant α is equal to 0.01. The field frequency is varied in the range 0–6 GHz to calculate the resonance spectra. The frequency step is 0.01 GHz near the resonance peaks and 0.1 GHz at the flat parts of the spectra. This algorithm of the simulation is successfully approved on modeling of FMR in Permalloy microstripes [30].

3. Results and discussion

3.1. Perpendicular anisotropy in the central spot

The resonance spectra and the spatial structure of the resonant modes in the UN state are represented in Fig. 2. The first mode (it means the mode having the lowest frequency, here and hereinafter) corresponds to the *quasi*-uniform oscillations of the magnetization in the central spot. The effective magnetic field determining the resonant frequency (Eq. (3)) of this mode has the lowest value as the anisotropy in the spot is less than in the surrounding film. Evidently the decrease of the anisotropy value in the spot from $K_1 = 2.8 \times 10^5$ erg/cm^3 to $K_1 = 2.4 \times 10^5$ erg/cm^3 leads to the shift of resonance to the lower frequency range (Fig. 2a). Actually this mode is *quasi*-uniform since the oscillation amplitude decays towards the area of the surrounding film (see the equation below). So addition of exchange field to the effective field exists. This addition is larger in the case of the smaller diameter of the central spot therefore the frequency of the first mode is shifted in the higher frequency range with the decrease of the spot diameter from 100 nm to 50 nm. The excitation of the series of the next modes is observed with the increase of the AC field frequency. They have a form of the standing spin waves with the radial symmetry confined in the central spot (Fig. 2b).

Since in the UN state the excited modes are centrosymmetric they can be described analytically. In the magnetostatic approximation (which should work well for the modes with the lower numbers) the equation of motion of magnetization can be solved in the Walker problem [28,31,32]. In this approximation the AC components of the magnetization have following spatial structure

$$m_x, m_y \sim J_\beta(k_\rho \rho) \cos\left(k_z z - \frac{1}{2}\eta\pi\right) \exp(i\beta\varphi). \tag{7}$$

Here ρ, φ, z are the cylindrical coordinates, J_β is the β-order Bessel function (β is an integer), $k_z^2 = -(1 + \xi(\omega))k_\rho^2$, χ is a high-frequency magnetic susceptibility, η is 0 or 1. The relation between k_ρ and k_z is obtained from the boundary conditions for the AC magnetic field at the surfaces of the sample. It links the field inside the sample to the corresponding exponentially decaying field outside the sample:

$$\tan\left(\frac{k_z h - \eta\pi}{2}\right) = \frac{k_\rho}{k_z}. \tag{8}$$

In order to obtain the uniform in z-direction modes, we take $\eta = 0$. Besides, for small film thickness h ($k_z h \ll 1$) we can take $\cos(k_z z) \approx 1$. We consider the φ-independent centrosymmetric modes with $\beta = 0$. So the components of magnetization take the form of

$$m_x, m_y \sim J_0(k_\rho \rho). \tag{9}$$

If the AC magnetization outside the circular spot is roughly estimated as zero the magnetization can be considered as pinned at the boundary of the disk. This leads to the equation $J_0\left(\frac{k_\rho d}{2}\right) = 0$ for k_ρ. Thus the n-th mode is determined by the n-th zero of the J_0 Bessel function. Indeed, each subsequent mode has one more circular peak in the numerical simulations; the number of the peaks corresponds to the mode number. The mode frequency can be estimated as

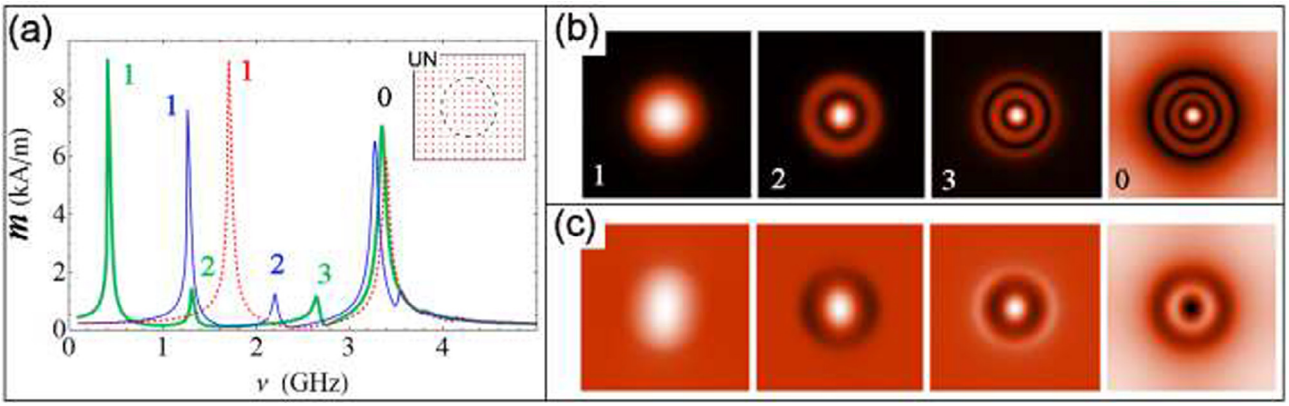

Fig. 2. (a) Thin blue line is FMR spectrum for the uniform (UN) state (shown in the inset) calculated for the system with $d = 100$ nm, $l = 200$ nm, $K_0 = 3.65 \times 10^5$ erg/cm^3, $K_1 = 2.8 \times 10^5$ erg/cm^3; thick green line is for the system with slightly reduced anisotropy in the central spot ($K_1 = 2.4 \times 10^5$ erg/cm^3); dashed red line is for the system with twice reduced scales ($d = 50$ nm, $l = 100$ nm). (b) The spatial structure of the modes for different resonant peaks denoted by the same numbers. The distribution of the amplitude of the AC magnetization in the system is shown. (c) is the snapshots of the x-component of the AC magnetization. (For interpretation of the references to colour in this figure legend, the reader is referred to the web version of this article.)

$$\nu_n = 2\gamma M_s(1+K_0/2\pi)\sqrt{1-(1+K_0/2\pi)^{-1}\left(1+2/hk_\rho^{(n)}\right)^{-1}}, \quad (10)$$

in the approximation $k_z h \ll 1$. Here $k_\rho^{(n)}$ corresponds to the n-th zero of Bessel function. This estimation shows that the frequency grows with the increase of the mode number. The formula (10) gives 1.26 GHz for the first mode which is in good agreement to the modeling (see Fig. 2). The higher order resonant modes have the larger exchange energy, which sufficiently shifts their frequencies to the higher band, so, the estimation (10) cannot be used in last case. The slight deviations of the mode structure from the radial symmetry observed in the simulations are caused by the square symmetry of the simulated elementary cell and by the fact that the exiting AC field is linearly polarized in the system plain.

Further increase of the AC field frequency leads to the excitations of the magnetization oscillations in the film out of the modified spot. This frequency can be roughly estimated as

$$\nu = \frac{\gamma}{2\pi}\left(\frac{2K_0}{M_s} - 2M_s\right), \quad (11)$$

which is approximately equal to 3.24 GHz for our material parameters. We denote this mode as the 0-mode since it corresponds to the quasi-uniform oscillations of the magnetization in the film. These quasi-uniform oscillations are accompanied by the radial standing wave in the central spot. The number of the radial peaks in these affiliated oscillations corresponds to the number of the highest confined mode. As the frequency of the 0-mode is primarily determined by the anisotropy field in the film it is practically independent on the geometry parameters of the system. The small peaks to the right of the 0-mode peak correspond to the nonuniform oscillations of the outer film (accompanied by some nonuniform oscillations of the central spot space). We do not present corresponding pictures as the oscillation amplitude is significantly small.

So the resonance modes in the case of the UN state can be classified as confined in the central spot and delocalized. The number of the confined modes increases with the increase of the central spot diameter.

The confined modes can have longer wave length in the increased spot, so the corresponding exchange fields decreases which leads to the shift of the mode frequencies to the lower band.

The same way the number of the confined modes increases with the decrease of the anisotropy value in the central area. The latter is the result of the dependence of the resonant frequencies on the anisotropy constant in a way similar to (11). This dependence is obviously provided by the change of the anisotropy energy.

The MB state (Fig. 1) has a more complicated distribution of the magnetization than the UN state as there is a Bloch type domain wall at the boundary of the central spot. The resonance spectra of the MB state and the structure of the modes are represented in Fig. 3. Whereas the resonance modes can also be classified as confined in the spot or delocalized in this case a new type of the confined oscillations appears in the system. These are the oscillations of the domain wall. There are two modes associated primarily with the oscillations of the magnetization within the domain wall. They are denoted by 1 and 2 in Fig. 3. Unlike the UN state the MB state does not have the radial symmetry. The symmetry break is explained by the fact that the magnetization in the MB state has the φ-component of curl **M** (Fig. 1c). In these conditions the oscillations are not the standing waves, they travel making complete revolution during the period of the oscillation.

$$m_x, m_y \sim \exp(i\beta\omega), \quad (12)$$

where φ is the azimuthal coordinate, β is an integer that has the meaning of the azimuthal wavenumber. The direction of rotation (i.e. the sign of β for each mode) is defined by the magnetostatic interaction (see [28]). In the first mode the spin wave propagates in the clockwise direction while in the second mode it travels in the opposite direction (see Fig. 3).

The magnetization oscillations of the inner part of the central spot are observed at the higher frequencies. The number of these confined modes depends on the spot diameter and the difference in the anisotropy values K_0 and K_1 as in the case of the UN state. The wider central spot can confine larger number of the modes. These oscillations also involve the area of the domain wall. Therefore they are not the radial standing waves like in UN state, but have the tangential inhomogeneity and are rotated (3 and 4 in Fig. 3b,c). Our simulations demonstrate that the direction of the rotation does not depend on the skyrmion helicity (i.e. on the direction of the magnetic moment in the domain wall [33]) of the MB. It depends on the toroidal moment density (φ-component of curl **M**). If one changes the direction of themagnetization in the MB and in the outer film to the opposite (which corresponds to the change of the skyrmion charge of the state from +1 to −1) the value $(\text{curl}\,\mathbf{M})_\varphi$ changes sign too. All the modes 1–4 change the directions of their rotation in this case. For considered material and geometrical parameters we observe only four confined modes. Like in the UN state these delocalized oscillations in the outer film are accompanied with the highest confined mode in the spot.

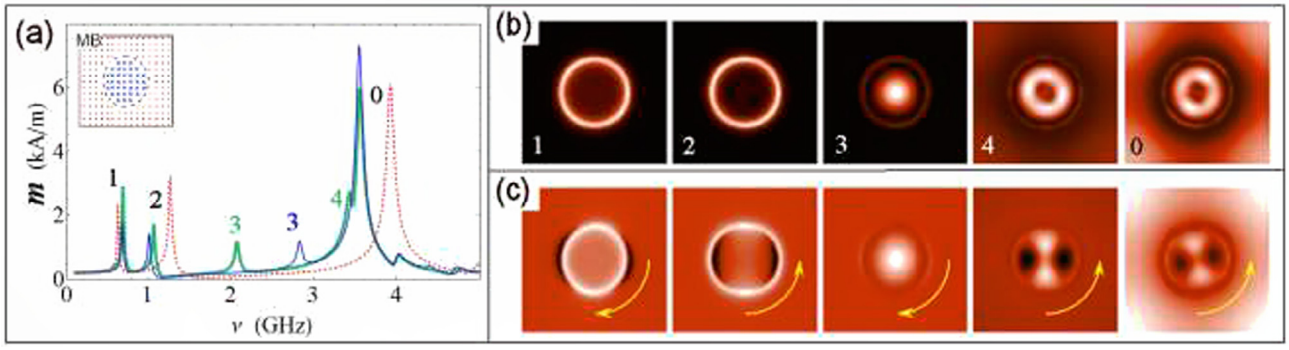

Fig. 3. (a) Thin blue solid line is FMR spectra for the magnetic bubble (MB) state (shown in the inset) calculated for the system with d = 100 nm, l = 200 nm, K_0 = 3.65 × 10^5 erg/cm^3, K_1 = 2.8 × 10^5 erg/cm^3; thick solid green line is for the system with slightly reduced anisotropy in the central spot (K_1 = 2.4 × 10^5 erg/cm^3); dashed red line is for the system with twice reduced scales (d = 50 nm, l = 100 nm). (b) The mode structures for different peaks denoted by the same numbers. The distributions of the amplitude of the AC magnetization in the system are shown. (c) The snapshots of the x-component of the AC magnetization. During the period of the oscillation the magnetization distributions make the complete revolution in the direction indicated by the arrows. (For interpretation of the references to colour in this figure legend, the reader is referred to the web version of this article.)

As the system can be easily switched between the UN and the MB state by the temporary applying of the appropriate external magnetic field [20,21] it is interesting to compare their FMR spectra in more detail. They are shown together in Fig. 4. The main difference in the spectra is the high peak corresponding to the uniform oscillations of the magnetization of the central spot in the UN state. Its intensity is comparable with the oscillations of the magnetization of the outer film (0-mode). The intensity of all other peaks is noticeably less.

3.2. In-plane anisotropy in the central spot

If the effective anisotropy of the central spot becomes of the easy plain type the formation of the vortex magnetization distribution in central spot is observed (Fig. 1) [20,21]. From the topological point of view the OV state is identical to the MB. Indeed if in MB state one fluently decreases the anisotropy in the central spot (K_1) the domain wall broadening and vortex core formation is observed.

We simulate the dynamic properties of the OV state for two sets of sizes with $K_1 = 10^5$ erg/cm^3. Those are $d = 100$ nm, $l = 200$ nm and $d = 50$ nm, $l = 100$ nm. The results are represented in Fig. 5. Similarly to the UN and the MB states we observe the modes confined in the central spot at the lower frequencies. Their number also increases with the diameter of the central spot. The first mode is the precession of the vortex core. For the second and successive modes the magnetization in the periphery of the vortex is also engaged into oscillations. All these confined oscillations are rotating spin waves. The first delocalized mode (0-mode) is the almost uniform precession of the magnetization in the outer film accompanied by the rotating spin-wave oscillations in the central spot. While the structure of the modes in the cases of the MB and the OV states is very different the modes having the same number rotate in the same direction defined by the sign of φ-component of curl **M**, which is the same for the MB and the OV. Another possible state in the case of the in-plain spot anisotropy is the co-directional vortex (Fig. 1b, OV). The FMR spectra and modes of OV are represented in Fig. 6. While OV is topologically identical to the UN state and does not have integral topological charge and toroidal moment, their local values are nonzero in this case. It leads to the fact that the oscillation modes retain their rotating nature. Let us compare the distribution of the $(\mathrm{curl}\,\mathbf{M})_\varphi$ and the structure of the modes in the OV and the CV cases (Figs. 1c, 5c, 6c).

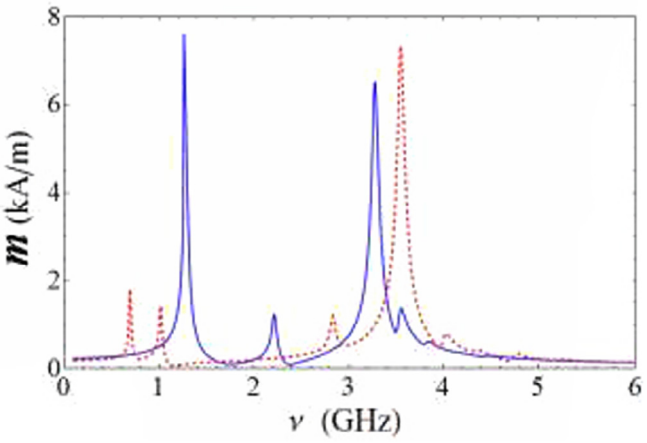

Fig. 4. Blue solid line is FMR spectrum of UN state calculated for the system with $d = 100$ nm, $l = 200$ nm, $K_0 = 3.65 \times 10^5$ erg/cm^3, $K_1 = 2.8 \times 10^5$ erg/cm^3; red dashed line is the FMR spectrum of MB state of the same system. (For interpretation of the references to colour in this figure legend, the reader is referred to the web version of this article.)

(i) In the low frequency modes 1, 2 and 3 (in Figs. 5 and 6) the oscillations primarily involve the magnetization in the central part of the spot near the vortex. OV and CV have the opposite values of the $(\mathrm{curl}\,\mathbf{M})_\varphi$ in the vortex core. Correspondingly these modes demonstrate rotation in the opposite directions for OV and CV.

(ii) In the higher frequency modes the oscillations of the magnetization have large amplitude near the boundary of the central spot. The local density of the toroidal moment $(\mathrm{curl}\,\mathbf{M})_\varphi$ has the same sign for OV and CV in the area of the inner 90° domain wall. So the modes 4, 5, 6 (Figs. 5 and 6) are rotated in the same direction in OV and CV.

The difference between the OV and the CV spectra is less than for the UN - MB pair of states. The reason is the fact that the noticeably larger volume of the sample changes its magnetization direction in the UN ⇔ MB transition than in the case of the vortex states (OV ⇔ CV), as the volume of the core is sufficiently small. Nevertheless we observe some shift of the resonance frequency of the core precession mode (1-mode) in the OV state if one decreases the diameter of the central spot (Fig. 5a). The effect is much less for the CV configuration. We can suggest the following explanation of such behavior. In the case of the OV state the magnetization of the core and the outer film is oppositely directed. The exchange energy is proportional to the gradients of the magnetization components $E \sim (\partial\mathbf{M}/\partial x_i)^2$. The decrease of the central spot diameter leads to the increase of thegradients. So the effective magnetic field

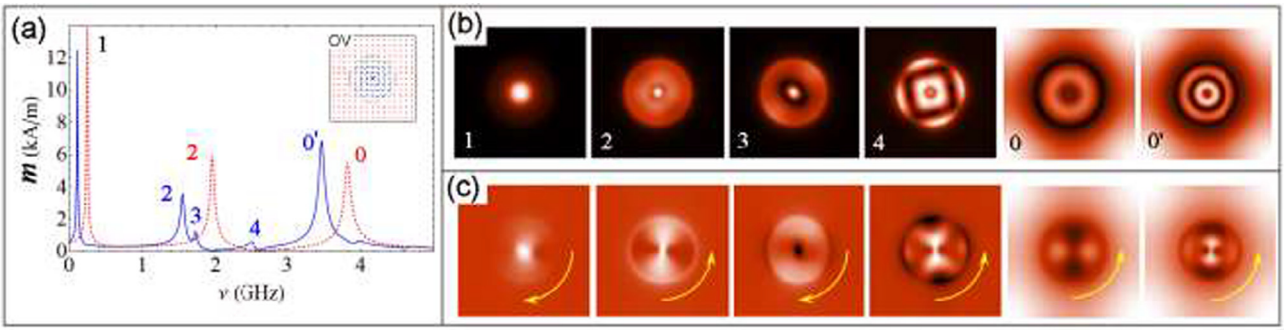

Fig. 5. (a) Blue solid line is FMR spectrum for the opposite vortex (OV) state (shown in the inset) calculated for the system with $d = 100$ nm, $l = 200$ nm, $K_0 = 3.65 \times 10^5$ erg/cm^3, $K_1 = 10^5$ erg/cm^3; red line dashed is for the system with twice reduced scales ($d = 50$ nm, $l = 100$ nm). (b) The mode structures for different peaks denoted by the same numbers. The distributions of the amplitude of the AC magnetization in the system are shown. (c) The snapshots of the x-component of the AC magnetization. During the period of the oscillation the magnetization distributions made the complete revolution in the directions indicated by the arrows. (For interpretation of the references to colour in this figure legend, the reader is referred to the web version of this article.)

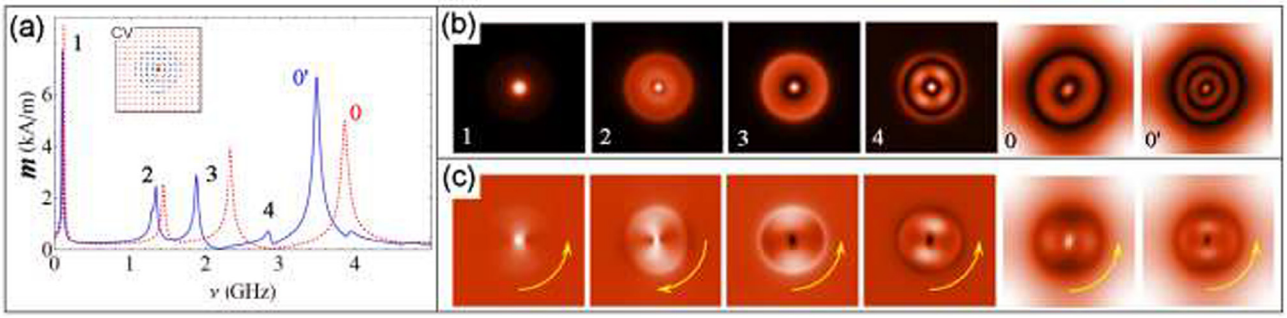

Fig. 6. (a) Blue solid line is FMR spectrum for the co-directional vortex (CV) state (shown in the inset) calculated for the system with $d = 100$ nm, $l = 200$ nm, $K_0 = 3.65 \times 10^5$ erg/cm^3, $K_1 = 10^5$ erg/cm^3; red dashed line is for the system with twice reduced scales ($d = 50$ nm, $l = 100$ nm). At the right; the mode structures for different peaks denoted by the same numbers. (b) The distributions of the amplitude of the AC magnetization in the system. (c) The snapshots of the x-component of the AC magnetization. During the period of the oscillation the magnetization distributions made the complete revolution in the direction indicated by the arrows. (For interpretation of the references to colour in this figure legend, the reader is referred to the web version of this article.)

is also increases and the resonance is shifted to the higher frequency range. In the case of the CV state the magnetization of the core and the outer film is codirectional and CV is topologically identical to the uniformly magnetized state UN. So if one decreases the central spot diameter the magnetization of the vortex shell has possibility to rise out of the plain in the z-direction to decrease exchange energy. The effective field is increased not so much in this case and the shift of the resonance is less.

4. Conclusion

Thus we analyze the FMR spectra in the magnetic film with the spatially modulated value of the perpendicular anisotropy. Both topologically charged and uncharged states are examined. It is found that the resonances in the spectra can be classified as localized and delocalized modes. The FMR spectra can be tuned by changing the geometrical parameters as well as changing material parameters of the system that can be easily done using the modern nanostructuring technologies [21]. Such systems with switching of magnetic states under external magnetic field (accompanied with changes in FMR spectra) can be used in the new generation of tunable microwave devices.

Acknowledgments

This research is supported by the Russian Science Foundation (Grant No. 16-12-10254).

Appendix A. Supplementary data

Supplementary data associated with this article can be found, in the online version, at http://dx.doi.org/10.1016/j.jmmm.2017.09.006.

References

[1] I.E. Dzyaloshinskii, B.A. Ivanov, JETP Lett. 29 (1979) 540.
[2] A.S. Kovalev, A.M. Kosevich, K.V. Maslov, JETP Lett. 30 (1979) 296.
[3] S. Muhlbauer, B. Binz, F. Jonietz, C. Pfleiderer, A. Rosch, A. Neubauer, R. Georgii, P. Boni, Science 323 (2009) 915.
[4] X.Z. Yu, Y. Onose, N. Kanazawa, J.H. Park, J.H. Han, Y. Matsui, N. Nagaosa, Y. Tokura, Nature (London) 465 (2010) 901.
[5] S. Heinze, K. von Bergmann, M. Menze, J. Brede, A. Kubetzka, R. Wiesendanger, G. Bihlmayer, S. Blugel, Nat. Phys. 7 (2011) 713.
[6] Y. Onose, N. Takeshita, C. Terakura, H. Takagi, Y. Tokura, Phys. Rev. B 72 (2005) 224431.
[7] A. Neubauer, C. Pfleiderer, B. Binz, A. Rosch, R. Ritz, P.G. Niklowitz, P. Boni, Phys. Rev. Lett. 102 (2009) 186602.
[8] B. Binza, A. Vishwanath, Physica B 403 (2008) 1336.
[9] M. Lee, W. Kang, Y. Onose, Y. Tokura, N.P. Ong, Phys. Rev. Lett. 102 (2009) 186601.
[10] F. Jonietz, S. Muhlbauer, C. Pfleiderer, A. Neubauer, W. Munzer, A. Bauer, T. Adams, R. Georgii, P. Boni, R.A. Duine, K. Everschor, M. Garst, A. Rosch, Science 330 (2010) 1648.
[11] X.Z. Yu, N. Kanazawa, W.Z. Zhang, T. Nagai, T. Hara, K. Kimoto, Y. Matsui, Y. Onose, Y. Tokura, Nat. Commun. 3 (2012) 988.
[12] S. Seki, S. Ishiwata, Y. Tokura, Phys. Rev. B 86 (2012) 060403.
[13] A. Fert, V. Cros, J. Sampaio, Nat. Nanotechnol. 8 (2013) 152.
[14] Y. Dai, H. Wang, T. Yang, W. Ren, Z. Zhang, Sci. Rep. 4 (2014) 6153.
[15] K.-W. Moon, D.-H. Kim, S.-G. Je, B.S. Chun, W. Kim, Z.Q. Qiu, S.-B. Choe, C. Hwang, Sci. Rep. 6 (2016) 20360.
[16] A. Bogdanov, A. Hubert, J. Magn. Magn. Mater. 138 (1994) 255.
[17] A. Bogdanov, A. Hubert, J. Magn. Magn. Mater. 195 (1999) 182.
[18] H.Y. Kwon, K.M. Bu, Y.Z. Wu, C. Won, J. Magn. Magn. Mater. 324 (2012) 2171.
[19] M.V. Sapozhnikov, O.L. Ermolaeva, Phys. Rev. B 91 (2015) 024418.
[20] M.V. Sapozhnikov, J. Magn. Magn. Mater. 396 (2015) 338.
[21] M.V. Sapozhnikov, S.N. Vdovichev, O.L. Ermolaeva, N.S. Gusev, A.A. Fraerman, S.A. Gusev, Yu.V. Petrov, Appl. Phys. Lett. 109 (2016) 042406.
[22] E. Nazaretski, J.D. Thompson, D.V. Pelekhov, T. Mewes, P.E. Wigen, J. Kim, M. Zalalutdinov, J.W. Baldwin, B. Houston, P.C. Hammel, R. Movshovich, J. Magn. Magn. Mater. 310 (2007) e941.
[23] B. Pigeau, C. Hahn, G. de Loubens, V.V. Naletov, O. Klein, K. Mitsuzuka, D. Lacour, M. Hehn, S. Andrieu, F. Montaigne, Phys. Rev. Lett. 109 (2012) 247602.
[24] I. Lee, Yu. Obukhov, G. Xiang, A. Hauser, F. Yang, P. Banerjee, D.V. Pelekhov, P.C. Hammel, Nature 466 (2010) 845.
[25] M.J. Donahue, D.G. Porter, OOMMF User's Guide Version 1.0, National Institute of Standards and Technology, Gaithersburg, MD, 1999.
[26] E.D. Boerner, H.N. Bertran, IEEE Trans Magn. 33 (1997) 3052.
[27] A.A. Fraerman, I.M. Nefedov, I.R. Karetnikova, M.V. Sapozhnikov, I.A. Shereshevskii, Phys. Met. Metallogr. 92 (Suppl. 1) (2001) 226.
[28] R.W. Damon, J.R. Eshbach, J. Phys. Chem. Solids 19 (1961) 308.
[29] E.A. Karashtin, A.A. Fraerman, Phys. Rev. B 92 (2015) 014401.
[30] E.V. Skorohodov, R.V. Gorev, R.R. Yakubov, E.S. Demidov, Yu.V. Khivintsev, Yu. A. Filimonov, V.L. Mironov, J. Magn. Magn. Mater. 424 (2017) 118.
[31] L.R. Walker, Phys. Rev. 105 (1957) 390.
[32] M. Sparks, Solid State Commun. 8 (1970) 731.
[33] N. Nagaosa, Y. Tokura, Nat. Nanotech. 8 (2013) 899.